

## PALEOCLIMATOLOGY

# Quantification of drought during the collapse of the classic Maya civilization

Nicholas P. Evans<sup>1\*</sup>, Thomas K. Bauska<sup>1</sup>, Fernando Gázquez-Sánchez<sup>1</sup>, Mark Brenner<sup>2</sup>, Jason H. Curtis<sup>2</sup>, David A. Hodell<sup>1</sup>

The demise of Lowland Classic Maya civilization during the Terminal Classic Period (~800 to 1000 CE) is a well-cited example of how past climate may have affected ancient societies. Attempts to estimate the magnitude of hydrologic change, however, have met with equivocal success because of the qualitative and indirect nature of available climate proxy data. We reconstructed the past isotopic composition ( $\delta^{18}\text{O}$ ,  $\delta\text{D}$ ,  $^{17}\text{O}$ -excess, and d-excess) of water in Lake Chichancanab, Mexico, using a technique that involves isotopic analysis of the structurally bound water in sedimentary gypsum, which was deposited under drought conditions. The triple oxygen and hydrogen isotope data provide a direct measure of past changes in lake hydrology. We modeled the data and conclude that annual precipitation decreased between 41 and 54% (with intervals of up to 70% rainfall reduction during peak drought conditions) and that relative humidity declined by 2 to 7% compared to present-day conditions.

More than two decades ago, a sediment core from Lake Chichancanab (Yucatán Peninsula, Mexico; fig. S1) provided the first physical evidence of a temporal correlation between drought and the sociopolitical transformation of the Classic Maya civilization during the Terminal Classic Period (TCP) (1). The presence of gypsum horizons and a concomitant increase in the oxygen isotope ratio ( $^{18}\text{O}/^{16}\text{O}$ ) in shells of ostracods and gastropods suggested the TCP was among the driest periods of the Holocene in northern Yucatán. Paleoclimate records produced subsequently provided additional evidence for drought during the TCP (2–9), but the magnitude of hydro-climate change and its influence on Maya agricultural and socio-political systems remains controversial (10). The qualitative nature of most climate proxy archives, combined with dating uncertainties, has prevented detailed assessment of the relationship between past climate and cultural changes (10–12).

Recent attempts to quantify estimates of past changes in rainfall amount and assess the impact on ancient Maya agriculture have used isotopes of either oxygen ( $\delta^{18}\text{O}$ ) (6, 13) or hydrogen ( $\delta\text{D}$ ) (9–11). No study to date has combined the two isotope systems, because the materials used for analysis (i.e., carbonates and leaf waxes) preclude simultaneous measurement of the multiple isotopologs of water. Combined analysis of  $\delta^{18}\text{O}$ ,  $\delta^{17}\text{O}$ , and  $\delta\text{D}$  is a powerful method to estimate past hydrologic changes quantitatively because hydrogen and triple oxygen isotopes each undergo

slightly different fractionation during evaporation, leading to changes in the derived d-excess [ $\delta\text{D} - (8 \times \delta^{18}\text{O})$ ] and  $^{17}\text{O}$ -excess [ $\ln(\delta^{17}\text{O} + 1) - 0.528 \ln(\delta^{18}\text{O} + 1)$ ] parameters (14–19). In an effectively closed hydrological basin such as Lake Chichancanab, the primary controls on the isotopic fractionation of lake water during evaporation include the fractional loss of precipitation to evaporation (P/E), normalized relative humidity ( $\text{RH}_n$ ), temperature, and changes in the precipitation source (1–3, 14). The value of d-excess is largely dependent on  $\text{RH}_n$  and temperature, whereas  $^{17}\text{O}$ -excess is controlled mainly by  $\text{RH}_n$  (14–19). Because the predicted trends of d-excess and  $^{17}\text{O}$ -excess in evaporating waters display different responses to climate variables, they can be evaluated individually using an iterative model (20).

We took advantage of the benefits of using all isotopologs of water and their derived parameters (d-excess and  $^{17}\text{O}$ -excess) by measuring triple oxygen and hydrogen isotopes in the hydration water of gypsum ( $\text{CaSO}_4 \cdot 2\text{H}_2\text{O}$ ) in sediment cores from Lake Chichancanab (fig. S2) (3). Today, the lake water is near saturation for gypsum; during past periods of drier climate, when the lake volume shrank, gypsum precipitated from the lake water and was preserved as distinct layers within the accumulating sediments (1–3). When gypsum forms, water molecules are incorporated directly into its crystalline structure, and this “gypsum hydration water” (GHW) records the isotopic composition of the parent fluid, with known isotopic fractionations (14, 17, 21–26). Unlike oxygen isotope fractionation during formation of carbonate minerals (27, 28), fractionation during gypsum crystallization is practically independent of temperature (24) or biological and kinetic (non-equilibrium) effects (17). Addi-

tionally, isotopes of GHW that are measured in the sedimented gypsum inherently record the driest periods, offering a distinct advantage over other traditional climate archives such as speleothems or mollusk shells, which may fail to register peak drought conditions because of growth hiatuses. Absolute differences in  $\delta^{18}\text{O}$ ,  $\delta\text{D}$ ,  $^{17}\text{O}$ -excess, and d-excess values between modern and paleo-lake water provide an estimate of differences between the lake hydrologic budget during the TCP and today (Fig. 1). Results were evaluated using a numerical isotope mass balance model that must satisfy all isotope variables (20) (fig. S3), and thus provides a more robust constraint on past hydrology than does modeling  $\delta^{18}\text{O}$  or  $\delta\text{D}$  alone.

The modern climate around Lake Chichancanab is characterized by a mean annual precipitation of ~1200 mm, a mean annual surface water temperature of ~26°C, and a net annual water deficit of 300 to 400 mm/year (3, 22). Large changes in precipitation and  $\text{RH}_n$  occur between the dry season (November to May) and the rainy season (June to October) (13, 29). Measured  $\delta^{18}\text{O}$  and  $\delta\text{D}$  of precipitation and groundwater samples from the Yucatán Peninsula, collected from 1994 to 2010, define a local meteoric water line (LMWL) with a slope of 7.7 (Fig. 2). Evaporation enriches the lake in the heavier isotopes of oxygen and hydrogen in water [ $2.6 \text{ per mil (‰)} < \delta^{18}\text{O} < 3.8\text{‰}$  and  $10.1\text{‰} < \delta\text{D} < 17.2\text{‰}$ ], evolving along an evaporative line defined by  $\delta\text{D} = (5.1 \times \delta^{18}\text{O}) - 3.1$ . This evaporation line intersects the LMWL at  $\delta^{18}\text{O} = -4.7(\pm 1.2)\text{‰}$  and  $\delta\text{D} = -27.5(\pm 10.7)\text{‰}$ , which is within error of the mean oxygen and hydrogen isotope values recorded in local rivers and groundwater from the International Atomic Energy Agency's regional Global Network of Isotopes in Precipitation stations ( $\delta^{18}\text{O} = -4.1\text{‰}$ ,  $\delta\text{D} = -24.3\text{‰}$ ) (29) and this study ( $\delta^{18}\text{O} = -4.0\text{‰}$ ,  $\delta\text{D} = -23.5\text{‰}$ ).

The gypsum deposited during the droughts of the Terminal Classic and early Postclassic periods was used to calculate  $\delta^{18}\text{O}$ ,  $\delta^{17}\text{O}$ , and  $\delta\text{D}$  values of the paleo-lake water, which ranged from  $3.6\text{‰}$  to  $4.9\text{‰}$  for  $\delta^{18}\text{O}$ ,  $1.9\text{‰}$  to  $2.5\text{‰}$  for  $\delta^{17}\text{O}$ , and  $13.7\text{‰}$  to  $18.8\text{‰}$  for  $\delta\text{D}$  (Fig. 1). Mean values of the paleo-lake waters ( $\delta^{18}\text{O} = 4.2\text{‰}$ ,  $\delta^{17}\text{O} = 2.2\text{‰}$ ,  $\delta\text{D} = 16.4\text{‰}$ ) during drought episodes are significantly greater than modern lake values ( $\delta^{18}\text{O} = 3.1\text{‰}$ ,  $\delta^{17}\text{O} = 1.6\text{‰}$ ,  $\delta\text{D} = 12.7\text{‰}$ ). Age uncertainty associated with the lake record and with periods of gypsum precipitation was calculated using Bayesian age-depth analysis of radiocarbon ages obtained from the sediment cores (3) (Fig. 1). We found high probabilities of drought occurring specifically during the onset (~750 to ~850 CE) and the end (~950 to ~1050 CE) of the TCP ( $P > 0.85$  and  $P > 0.95$ , respectively) (20). Multiple proxy climate records across the Maya Lowlands also provide evidence of drought synchronicity, with only slight temporal variations across the region (10).

To estimate quantitatively the magnitude of drought during the TCP, we used a transient model that explicitly simulates the evolution of the isotopic and chemical composition of the

<sup>1</sup>Godwin Laboratory for Palaeoclimate Research, Department of Earth Sciences, University of Cambridge, Cambridge CB2 3EQ, UK. <sup>2</sup>Department of Geological Sciences, University of Florida, Gainesville, FL 32611, USA.

\*Corresponding author. Email: ne243@cam.ac.uk

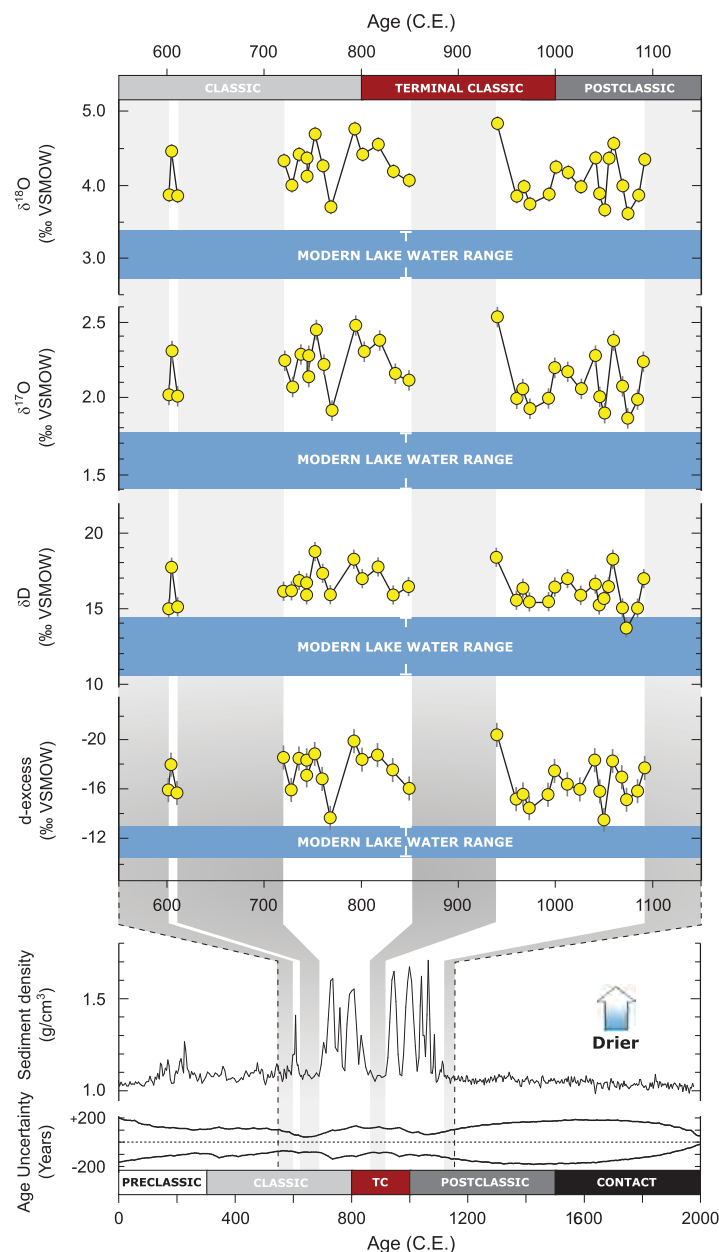


**Fig. 1. Water isotopes during drought periods compared to modern water isotopes of Lake Chichancanab.** Lower panel: Sediment density record of core CH1 7-III-04 from 0 to 2000 CE (shown relative to Maya chronology) (3). Periods of gypsum precipitation are indicated by density values of  $>1.1 \text{ g/cm}^3$ . Age uncertainties (95% confidence intervals) are derived from Bayesian age-depth analysis and normalized to the best-fit age model (20) (fig. S8). Upper panel:  $\delta^{18}\text{O}$ ,  $\delta^{17}\text{O}$ ,  $\delta\text{D}$ , and d-excess [d-excess =  $\delta\text{D} - (8 \times \delta^{18}\text{O})$ ] of paleo-lake water data (yellow circles) from 550 to 1150 CE shown after correction of measured GHW for known fractionation factors (24) at  $26^\circ\text{C}$ . Horizontal blue bands define the mean ( $\pm 1\sigma$ ) isotopic compositions recorded in the modern lake. Positive  $\delta^{18}\text{O}$ ,  $\delta^{17}\text{O}$ , and  $\delta\text{D}$  values and negative d-excess values reflect periods of drought. Note that the d-excess axis is reversed. VSMOW, Vienna Standard Mean Ocean Water.

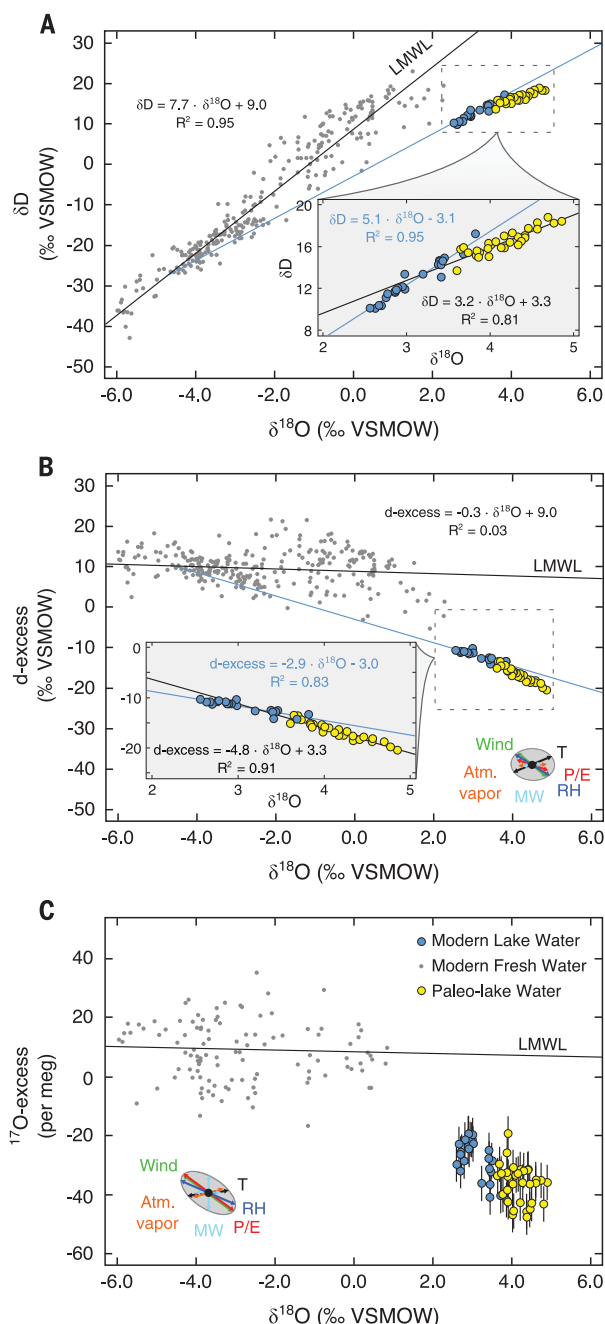


**Fig. 2. Comparison of measured local meteoric water, modern lake water, and paleo-lake water data.** Paleo-lake water data (yellow circles) are shown after correction of measured GHW for known fractionation factors (24) at  $26^\circ\text{C}$ . (A)  $\delta^{18}\text{O}$  versus  $\delta\text{D}$  space. (B)  $\delta^{18}\text{O}$  versus d-excess space. (C)  $\delta^{18}\text{O}$  versus  $^{17}\text{O}$ -excess space [ $^{17}\text{O}$ -excess =  $\ln(\delta^{17}\text{O} + 1) - 0.528 \ln(\delta^{18}\text{O} + 1)$ ]. Local meteoric water measurements (gray circles) define the local meteoric water line (LMWL). Relative to modern lake waters (blue circles), paleo-lake water displays greater  $\delta^{18}\text{O}$  and  $\delta\text{D}$  values along an evaporative trend. The gray ellipses define the relative influence of variables that can affect the isotopic composition of water in  $\delta^{18}\text{O}$  versus d-excess and  $\delta^{18}\text{O}$  versus  $^{17}\text{O}$ -excess space; the effects of precipitation/evaporation (P/E), normalized relative humidity ( $\text{RH}_n$ ), temperature (T), changes to source composition (MW), the degree of equilibrium between atmospheric vapor and fresh water (Atm. vapor), and turbulence created by wind are indicated (14). The size of each arrow is derived from the tolerance given for each input parameter in table S8.

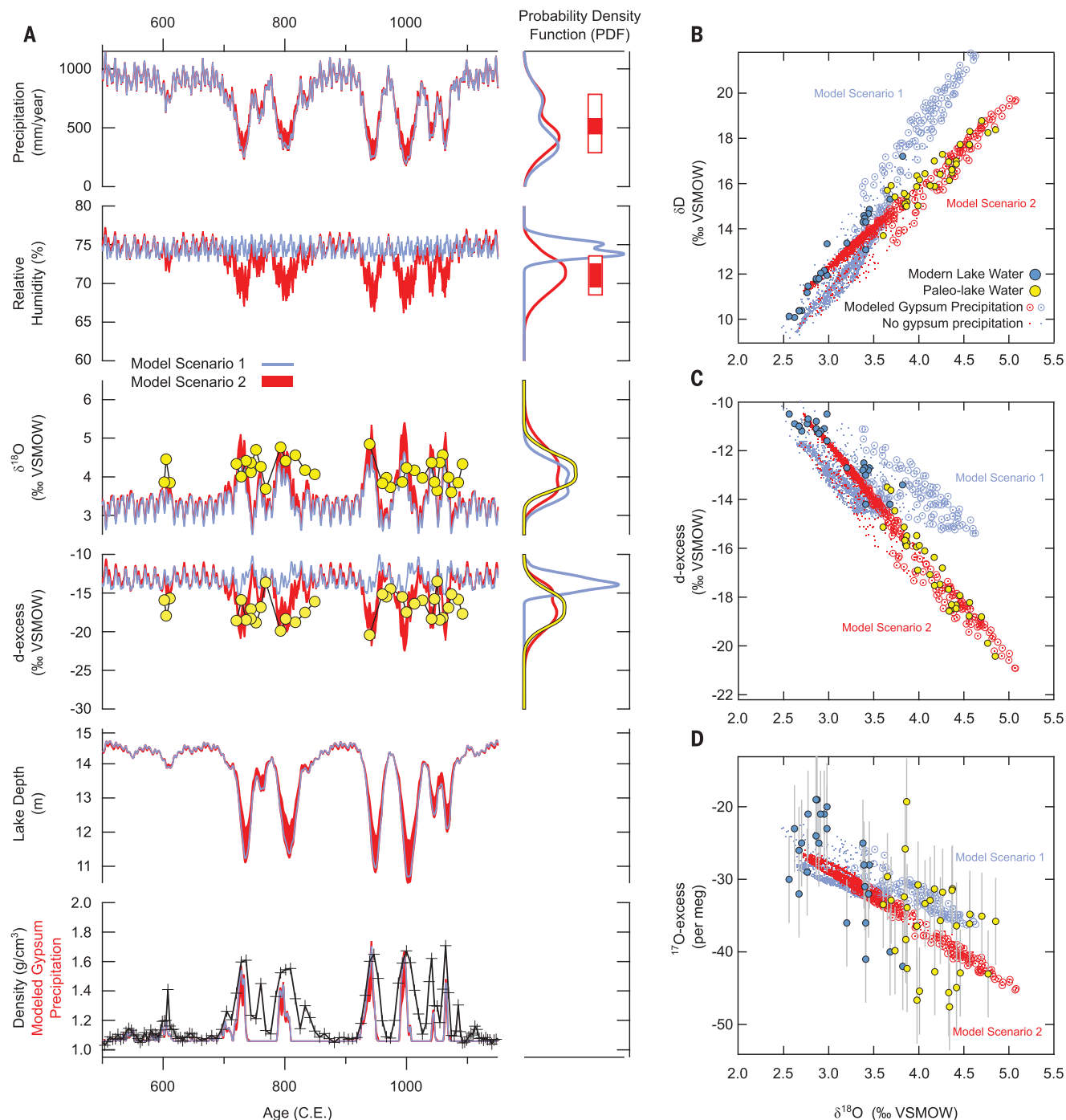


**Fig. 3. Simulated hydrologic changes of Lake Chichancanab.** (A) Transient model of the lake system from 550 to 1200 CE. GHW data (yellow circles) and core density are plotted against sampling ages derived from Bayesian age-depth analysis (20). Multidecadal-scale droughts were simulated by forcing (i) a reduction in precipitation with accompanied shifts in the isotopic composition of rainwater (i.e., the amount effect:  $\delta^{18}\text{O}_{\text{precipitation}}/\Delta\text{precipitation}_{\text{volume}} = -0.0121\text{‰/mm}$ ; scenario 1, blue line) and (ii) reductions in precipitation with accompanied decreases in  $\text{RH}_n$  (scenario 2, red field). Probability density functions (PDFs) incorporate the variability within and between each decade-long drought (yellow line, GHW data; blue line, scenario 1; red line, scenario 2). Scenario 1 fails to match the d-excess data

derived from GHW. Scenario 2 successfully reproduces all  $\delta^{18}\text{O}$  and d-excess data. When all model variables are averaged across all droughts, the mean precipitation and  $\text{RH}_n$  reduction (solid red boxes adjacent to PDFs) is 47% (with a  $1\sigma$  level of 41 to 54%) and 4% ( $1\sigma$  level of 2 to 7%), respectively. The  $\pm 1\sigma$  range determined from PDFs (open red boxes adjacent to PDFs) shows the variability of precipitation and  $\text{RH}_n$  throughout the droughts. (B to D) Scenarios 1 and 2 are also plotted as  $\delta^{18}\text{O}$  versus  $\delta\text{D}$  (B),  $\delta^{18}\text{O}$  versus d-excess (C), and  $\delta^{18}\text{O}$  versus  $^{17}\text{O}$ -excess (D). Open circles indicate points in the model at which gypsum is precipitating; dots indicate modeled data points when gypsum is not precipitating. Error bars ( $\pm 1\sigma$ ) are shown or are smaller than the symbols.

lake water, including the gypsum flux to the lake sediments (fig. S3). The modeled gypsum flux can be compared to observed variations in the gypsum content of the sediments, as expressed by variations in sediment bulk density (3). Changes in lake surface area/volume ratio were obtained from the lake bathymetry (fig. S4). The model was run at submonthly resolution in a series of millennial-duration experiments, forced with North American Regional Reanalysis (NARR) data for local precipitation and  $RH_n$ . We first tested the model using the climate forcing across the modern sampling period from 1994 to 2010 (fig. S5). It successfully reproduced the mean of modern isotope data, with insignificant gypsum precipitation. This time interval, which was fortuitously one of the driest of recent decades, was then used as the baseline for comparison to paleo-simulations.

To provide scenarios that are directly comparable to the GHW data, we performed long transient simulations in which rainfall and  $RH_n$  were reduced by variable amounts to simulate a series of multidecadal-scale droughts. The use of a model allows us to compare, directly and quantitatively, climate conditions that affect the modern lake with conditions that would plausibly lead to drought. First, only the intervals over which the model produced gypsum deposition (modeled sediment density  $>1.1 \text{ g/cm}^3$ ) were selected. The periods of modeled gypsum accumulation were then aggregated into drought conditions for a given scenario via two pathways: (i) All model variables were averaged across all of the droughts, and (ii) probability density functions (PDFs) were constructed incorporating the variability within and between each decadal-length drought. Data-consistent scenarios were then selected by excluding those model runs that fell outside the  $1\sigma$  range of the isotope data and where, on average, the model failed to produce significant gypsum accumulation (cutoff of average density  $<1.2 \text{ g/cm}^3$  based on  $1\sigma$  range; fig. S6). Two possible scenarios were tested subsequently: (i) a reduction in precipitation with accompanying shifts in the isotopic composition of rainwater (i.e., the amount effect), and (ii) a reduction in precipitation with accompanying decreases in  $RH_n$  (Fig. 3).

In the first scenario, precipitation  $\delta^{18}\text{O}$  was reduced with an increase in rainfall according to the amount-effect relationship (i.e.,  $\delta^{18}\text{O}_{\text{precipitation}}/\Delta\text{precipitation}_{\text{volume}} = -0.0121\text{‰/mm}$ ; fig. S7) with associated changes in  $\delta\text{D}$  and  $\delta^{17}\text{O}$  that track the global MWL (i.e., no changes in d-excess or  $^{17}\text{O}$ -excess). No scenarios with these assumptions are able to reproduce the relationship among  $\delta^{18}\text{O}$ , d-excess, and  $^{17}\text{O}$ -excess observed in the data. If the constraints provided by d-excess and  $^{17}\text{O}$ -excess are removed and only  $\delta^{18}\text{O}$  and gypsum precipitation are used, our model permits reductions in precipitation that average 50% over all drought intervals (Fig. 3, blue lines). This estimate is in broad agreement with previous work that relied on carbonate  $\delta^{18}\text{O}$ -derived precipitation estimates (using the local amount effect), which predicted reductions of up to 40% (6, 13). Our greater estimate of 50% is in part a consequence of the

peak drought  $\delta^{18}\text{O}$  values recorded by gypsum, as well as the integration of simulated gypsum formation and true lake bathymetry in the model. Crucially, however, the added information from the d-excess and  $^{17}\text{O}$ -excess data suggests that multidecadal shifts in the  $\delta^{18}\text{O}$  of precipitation (caused by the amount effect) were not the dominant factor that affected the isotope budget of Lake Chichancanab during the TCP.

In the second scenario, we reduced precipitation without changes in the  $\delta^{18}\text{O}$  of precipitation, but instead with concurrent changes in  $RH_n$ . In this case, we observed excellent agreement in the modeled evolution of all isotopic data, with increases in  $\delta^{18}\text{O}$  accompanied by decreases in d-excess and  $^{17}\text{O}$ -excess (Fig. 3, red lines). This analysis yielded plausible scenarios of precipitation reduction that average 47% across all droughts (with a  $1\sigma$  level of 41 to 54%) accompanied by  $RH_n$  reductions of 4% ( $1\sigma$  level of 2 to 7%). This result provides a robust, quantitative estimate of the mean annual hydrological conditions of the combined drought periods during the TCP at Lake Chichancanab.

Although the time evolution of our model is not a direct reconstruction of climate conditions, the model permits heterogeneity within and between each decade-long drought. The  $\pm 1\sigma$  range determined from the PDFs indicates that the precipitation reduction could vary from 20 to 70% throughout the modeled droughts (Fig. 3). This variability represents the transition into and out of drought phases and demonstrates that the severity of the droughts could be intense (up to a 70% reduction in precipitation) while maintaining the isotope balance and without desiccating the lake. Although variability in the seasonal delivery of rainfall (or lack thereof) is difficult to constrain because the residence time of the lake water is greater than an annual cycle, our results provide quantitative estimates for the total annual reduction in the water available to the ancient Maya for agricultural and domestic use. Note that recorded Colonial-period accounts of later droughts (e.g., 1535–1560 and 1765–1773), during which high mortality, famines, and population displacement were reported (30), are not manifest as intervals of gypsum precipitation in Lake Chichancanab. The lack of gypsum formation is likely a result of shorter duration and/or lower severity of these droughts, providing further evidence that the TCP was an unusually dry period for the Holocene on the Yucatán Peninsula.

Using triple oxygen and hydrogen isotope data to independently deconvolve climate variables of precipitation,  $RH_n$ , and the amount effect, we constrained the changing hydrological conditions at Lake Chichancanab. This approach provides a substantial advance over previous attempts to estimate the magnitude of rainfall reduction during the TCP droughts [e.g., (6, 13)]. Furthermore, these quantitative estimates of past rainfall and  $RH_n$  can serve as input variables in crop models, thereby clarifying how drought affected agriculture (e.g., maize production) in the northern Maya Lowlands during the TCP (12).

## REFERENCES AND NOTES

1. D. A. Hodell, J. H. Curtis, M. Brenner, *Nature* **375**, 391–394 (1995).
2. D. A. Hodell, M. Brenner, J. H. Curtis, T. Guilderson, *Science* **292**, 1367–1370 (2001).
3. D. A. Hodell, M. Brenner, J. H. Curtis, *Quat. Sci. Rev.* **24**, 1413–1427 (2005).
4. J. H. Curtis, D. A. Hodell, M. Brenner, *Quat. Res.* **46**, 37–47 (1996).
5. G. H. Haug et al., *Science* **299**, 1731–1735 (2003).
6. M. Medina-Elizalde et al., *Earth Planet. Sci. Lett.* **298**, 255–262 (2010).
7. D. J. Kennett et al., *Science* **338**, 788–791 (2012).
8. D. Wahl, F. Estrada-Belli, L. A. Anderson, *Palaeogeogr. Palaeoclimatol. Palaeoecol.* **379–380**, 17–31 (2013).
9. P. M. Douglas et al., *Proc. Natl. Acad. Sci. U.S.A.* **112**, 5607–5612 (2015).
10. P. M. Douglas, A. A. Demarest, M. Brenner, M. A. Canuto, *Annu. Rev. Earth Planet. Sci.* **44**, 613–645 (2016).
11. P. M. Douglas, M. Brenner, J. H. Curtis, *Global Planet. Change* **138**, 3–24 (2016).
12. J. Yaeger, D. A. Hodell, in *El Niño, Catastrophism, and Culture Change in Ancient America*, D. H. Sandweiss, J. Quilter, Eds. (Harvard Univ. Press, 2008), pp. 187–242.
13. M. Medina-Elizalde, E. J. Rohling, *Science* **335**, 956–959 (2012).
14. F. Gázquez et al., *Earth Planet. Sci. Lett.* **481**, 177–188 (2018).
15. H. Craig, L. I. Gordon, in *Stable Isotopes in Oceanographic Studies and Paleotemperatures*, E. Tongiorgi, Ed. (Consiglio Nazionale Delle Ricerche, Laboratorio di Geologia Nucleare, Pisa, 1965), pp. 9–130.
16. J. R. Gat, *Annu. Rev. Earth Planet. Sci.* **24**, 225–262 (1996).
17. D. Herwartz, J. Surma, C. Voigt, S. Assonov, M. Staubwasser, *Geochim. Cosmochim. Acta* **209**, 254–266 (2017).
18. B. Luz, E. Barkan, *Geochim. Cosmochim. Acta* **74**, 6276–6286 (2010).
19. J. Surma, S. Assonov, M. J. Bolouchi, M. Staubwasser, *Geophys. Res. Lett.* **42**, 8456–8462 (2015).
20. See supplementary materials.
21. Z. Sofer, *Geochim. Cosmochim. Acta* **42**, 1141–1149 (1978).
22. D. A. Hodell et al., *Geochim. Cosmochim. Acta* **77**, 352–368 (2012).
23. N. P. Evans et al., *Earth Planet. Sci. Lett.* **430**, 499–510 (2015).
24. F. Gázquez, N. P. Evans, D. A. Hodell, *Geochim. Cosmochim. Acta* **198**, 259–270 (2017).
25. F. Gázquez, J. M. Calaforra, N. P. Evans, D. A. Hodell, *Chem. Geol.* **452**, 34–46 (2017).
26. F. Gázquez et al., *Rapid Commun. Mass Spectrom.* **29**, 1997–2006 (2015).
27. T. Kluge, H. P. Affek, *Quat. Sci. Rev.* **49**, 82–94 (2012).
28. M. S. Lachniet, *Quat. Sci. Rev.* **28**, 412–432 (2009).
29. L. I. Wassenaar, S. L. Van Wilgenburg, K. Larson, K. A. Hobson, *J. Geochem. Explor.* **102**, 123–136 (2009).
30. J. A. Hoggarth, M. Restall, J. W. Wood, D. J. Kennett, *Curr. Anthropol.* **58**, 82–113 (2017).

## ACKNOWLEDGMENTS

We thank J. Rolfe for technical assistance and support with stable isotope measurements, R. Medina-Gonzalez for logistical field support, and three anonymous reviewers for insightful comments that improved the paper. **Funding:** Supported by the European Research Council under the European Union's Seventh Framework Program (FP/2007-2013)/ERC grant agreement 339694 (Water Isotopes of Hydrated Minerals) (D.A.H.). **Author contributions:** D.A.H., N.P.E., and F.G.-S. developed the analytical method and designed the study; M.B., J.H.C., and D.A.H. collected the original sediment cores from Lake Chichancanab; N.P.E. sampled the cores; N.P.E. and F.G.-S. performed all isotopic analyses; T.K.B. designed the transient model and performed drought simulations; and N.P.E., T.K.B., and D.A.H. wrote the paper with contributions from all other authors. **Competing interests:** The authors declare no competing interests. **Data availability:** All data are available in the manuscript or supplementary materials, and at [www.ncdc.noaa.gov/paleo/study/24476](http://www.ncdc.noaa.gov/paleo/study/24476).

## SUPPLEMENTARY MATERIALS

[www.sciencemag.org/content/361/6401/498/suppl/DC1](http://www.sciencemag.org/content/361/6401/498/suppl/DC1)  
Materials and Methods  
Modeling  
Figs. S1 to S11  
Tables S1 to S10  
References (31–54)

27 March 2018; accepted 31 May 2018  
10.1126/science.aas9871